Shaping and spatiotemporal characterization of sub-10-fs pulses focused by a high-NA objective

Monika Pawłowska,[1,2] Sebastian Goetz,[1] Christian Dreher,[1] Matthias Wurdack,[1] Enno Krauss,[3] Gary Razinskas,[3] Peter Geisler,[3] Bert Hecht,[3,4] and Tobias Brixner[1,4,*]

[1]*Institut für Physikalische und Theoretische Chemie, Universität Würzburg, Am Hubland, 97074 Würzburg, Germany*
[2]*Nencki Institute for Experimental Biology, Polish Academy of Sciences, 3 Pasteur Street, 02-093 Warszawa, Poland*
[3]*Nano-Optics and Biophotonics Group, Experimentelle Physik 5, Universität Würzburg, Am Hubland, 97074 Würzburg, Germany*
[4]*Röntgen Center for Complex Material Systems (RCCM), Am Hubland, 97074 Würzburg, Germany*
**brixner@phys-chemie.uni-wuerzburg.de*

Abstract: We describe a setup consisting of a $4f$ pulse shaper and a microscope with a high-NA objective lens and discuss the aspects most relevant for an undistorted spatiotemporal profile of the focused beam. We demonstrate shaper-assisted pulse compression in focus to a sub-10-fs duration using phase-resolved interferometric spectral modulation (PRISM). We introduce a nanostructure-based method for sub-diffraction spatiotemporal characterization of strongly focused pulses. The distortions caused by optical aberrations and space–time coupling from the shaper can be reduced by careful setup design and alignment to about 10 nm in space and 1 fs in time.

OCIS codes: (180.3170) Interference microscopy; (180.5810) Scanning microscopy; (310.6628) Subwavelength structures, nanostructures; (320.5540) Pulse shaping; (320.7100) Ultrafast measurements.

References and links

1. M. Müller, J. Squier, B. Wolleschensky, U. Simon, and G. J. Brakenhoff, "Dispersion pre-compensation of 15 femtosecond optical pulses for high-numerical-aperture objectives," J. Microsc. **191**, 141–150 (1998).
2. J. Jasapara and W. Rudolph, "Characterization of sub-10-fs pulse focusing with high-numerical-aperture microscope objectives," Opt. Lett. **24**, 777–779 (1999).
3. B. Piglosiewicz, D. Sadiq, M. Mascheck, S. Schmidt, M. Silies, P. Vasa, and C. Lienau, "Ultrasmall bullets of light–focusing few-cycle light pulses to the diffraction limit," Opt. Express **19**, 14451–14463 (2011).
4. T. Hanke, G. Krauss, D. Träutlein, B. Wild, R. Bratschitsch, and A. Leitenstorfer, "Efficient nonlinear light emission of single gold optical antennas driven by few-cycle near-infrared pulses," Phys. Rev. Lett. **103**, 257404 (2009).
5. M. Kempe, U. Stamm, B. Wilhelmi, and W. Rudolph, "Spatial and temporal transformation of femtosecond laser pulses by lenses and lens systems," J. Opt. Soc. Am. B **9**, 1158–1165 (1992).
6. I. Pastirk, J. Dela Cruz, K. Walowicz, V. Lozovoy, and M. Dantus, "Selective two-photon microscopy with shaped femtosecond pulses," Opt. Express **11**, 1695–1701 (2003).
7. M. H. Brenner, D. Cai, J. A. Swanson, and J. P. Ogilvie, "Two-photon imaging of multiple fluorescent proteins by phase-shaping and linear unmixing with a single broadband laser," Opt. Express **21**, 17256–17264 (2013).
8. M. I. Stockman, "Ultrafast nanoplasmonics under coherent control," New Journal of Physics **10**, 025031 (2008).

#223677 - $15.00 USD Received 23 Sep 2014; revised 18 Nov 2014; accepted 20 Nov 2014; published 12 Dec 2014

9. M. Aeschlimann, T. Brixner, A. Fischer, C. Kramer, P. Melchior, W. Pfeiffer, C. Schneider, C. Strüber, P. Tuchscherer, and D. V. Voronine, "Coherent two-dimensional nanoscopy," Science **333**, 1723–1726 (2011).
10. M. Aeschlimann, M. Bauer, D. Bayer, T. Brixner, S. Cunovic, A. Fischer, P. Melchior, W. Pfeiffer, M. Rohmer, C. Schneider, C. Strüber, P. Tuchscherer, and D. V. Voronine, "Optimal open-loop near-field control of plasmonic nanostructures," New J. Phys. **14**, 033030 (2012).
11. P. Biagioni, D. Brida, J.-S. Huang, J. Kern, L. Du, B. Hecht, M. Finazzi, and G. Cerullo, "Dynamics of four-photon photoluminescence in gold nanoantennas," Nano Letters **12**, 2941–2947 (2012). PMID: 22551099.
12. C. Rewitz, G. Razinskas, P. Geisler, E. Krauss, S. Goetz, M. Pawłowska, B. Hecht, and T. Brixner, "Coherent control of plasmon propagation in a nanocircuit," Phys. Rev. Appl. **1**, 014007 (2014).
13. R. Hildner, D. Brinks, J. B. Nieder, R. J. Cogdell, and N. F. van Hulst, "Quantum coherent energy transfer over varying pathways in single light-harvesting complexes," Science **340**, 1448–1451 (2013).
14. M. Wefers and K. Nelson, "Space-time profiles of shaped ultrafast optical waveforms," IEEE J. Quant. Electron. **32**, 161–172 (1996).
15. C. Dorrer and F. Salin, "Phase amplitude coupling in spectral phase modulation," IEEE J. Sel. Top. Quant. Electron. **4**, 342–345 (1998).
16. J. Vaughan, T. Feurer, K. Stone, and K. Nelson, "Analysis of replica pulses in femtosecond pulse shaping with pixelated devices," Opt. Express **14**, 1314–1328 (2006).
17. B. J. Sussman, R. Lausten, and A. Stolow, "Focusing of light following a 4-f pulse shaper: Considerations for quantum control," Phys. Rev. A **77**, 043416–11 (2008).
18. F. Frei, A. Galler, and T. Feurer, "Space-time coupling in femtosecond pulse shaping and its effects on coherent control," J. Chem. Phys. **130**, 034302–14 (2009).
19. F. Frei, R. Bloch, and T. Feurer, "Influence of finite spatial resolution on single- and double-pass femtosecond pulse shapers," Opt. Lett. **35**, 4072–4074 (2010).
20. N. Krebs, R. A. Probst, and E. Riedle, "Sub-20 fs pulses shaped directly in the UV by an acousto-optic programmable dispersive filter," Opt. Express **18**, 6164–6171 (2010).
21. M. A. Coughlan, M. Plewicki, and R. J. Levis, "Spatio-temporal and -spectral coupling of shaped laser pulses in a focusing geometry," Opt. Express **18**, 23973–23986 (2010).
22. D. Brinks, R. Hildner, F. D. Stefani, and N. F. van Hulst, "Beating spatio-temporal coupling: implications for pulse shaping and coherent control experiments," Opt. Express **19**, 26486–26499 (2011).
23. C. Radzewicz, M. la Grone, and J. Krasinski, "Interferometric measurement of femtosecond pulse distortion by lenses," Opt. Commun. **126**, 185–190 (1996).
24. R. Netz, T. Feurer, R. Wolleschensky, and R. Sauerbrey, "Measurement of the pulse-front distortion in high-numerical-aperture optics," Appl. Phys. B **70**, 833–837 (2000).
25. P. Bowlan, P. Gabolde, and R. Trebino, "Directly measuring the spatio-temporal electric field of focusing ultrashort pulses," Opt. Express **15**, 10219–10230 (2007).
26. P. Bowlan, U. Fuchs, R. Trebino, and U. D. Zeitner, "Measuring the spatiotemporal electric field of tightly focused ultrashort pulses with sub-micron spatial resolution," Opt. Express **16**, 13663–13675 (2008).
27. T.-w. Wu, J. Tang, B. Hajj, and M. Cui, "Phase resolved interferometric spectral modulation (PRISM) for ultrafast pulse measurement and compression," Opt. Express **19**, 12961–12968 (2011).
28. C. Froehly, B. Colombeau, and M. Vampouille, "Shaping and analysis of picosecond light pulses," Prog. Optics **20**, 63–153 (1983).
29. A. M. Weiner, D. E. Leaird, J. S. Patel, and J. R. Wullert, "Programmable femtosecond pulse shaping by use of a multielement liquid-crystal phase modulator," Opt. Lett. **15**, 326–328 (1990).
30. M. M. Wefers and K. A. Nelson, "Generation of high-fidelity programmable ultrafast optical waveforms," Opt. Lett. **20**, 1047–1049 (1995).
31. A. M. Weiner, "Femtosecond pulse shaping using spatial light modulators," Rev. Sci. Instrum. **71**, 1929–1960 (2000).
32. A. Monmayrant, S. Weber, and B. Chatel, "A newcomer's guide to ultrashort pulse shaping and characterization," J. Phys. B: At. Mol. Opt. Phys. **43**, 103001 (2010).
33. T. Binhammer, E. Rittweger, R. Ell, F. Kartner, and U. Morgner, "Prism-based pulse shaper for octave spanning spectra," IEEE J. Quant. Electron. **41**, 1552–1557 (2005).
34. B. Xu, Y. Coello, V. V. Lozovoy, D. A. Harris, and M. Dantus, "Pulse shaping of octave spanning femtosecond laser pulses," Opt. Express **14**, 10939–10944 (2006).
35. C. Rewitz, T. Keitzl, P. Tuchscherer, S. Goetz, P. Geisler, G. Razinskas, B. Hecht, and T. Brixner, "Spectral-interference microscopy for characterization of functional plasmonic elements," Opt. Express **20**, 14632–14647 (2012).
36. L. Novotny and B. Hecht, *Principles of Nano-Optics* (Cambridge University Press, Cambridge, 2006).
37. I. Amat-Roldán, I. Cormack, P. Loza-Alvarez, E. Gualda, and D. Artigas, "Ultrashort pulse characterisation with SHG collinear-FROG," Opt. Express **12**, 1169–1178 (2004).
38. G. Stibenz and G. Steinmeyer, "Interferometric frequency-resolved optical gating," Opt. Express **13**, 2617–2626 (2005).
39. A. Galler and T. Feurer, "Pulse shaper assisted short laser pulse characterization," Appl. Phys. B **90**, 427–430

#223677 - $15.00 USD Received 23 Sep 2014; revised 18 Nov 2014; accepted 20 Nov 2014; published 12 Dec 2014

(2008).
40. Y. Coello, V. V. Lozovoy, T. C. Gunaratne, B. Xu, I. Borukhovich, C.-h. Tseng, T. Weinacht, and M. Dantus, "Interference without an interferometer: a different approach to measuring, compressing, and shaping ultrashort laser pulses," J. Opt. Soc. Am. B **25**, A140–A150 (2008).
41. D. Yelin, D. Meshulach, and Y. Silberberg, "Adaptive femtosecond pulse compression," Opt. Lett. **22**, 1793–1795 (1997).
42. T. Baumert, T. Brixner, V. Seyfried, M. Strehle, and G. Gerber, "Femtosecond pulse shaping by an evolutionary algorithm with feedback," Appl. Phys. B **65**, 779–782 (1997).
43. T. Brixner, M. Strehle, and G. Gerber, "Feedback-controlled optimization of amplified femtosecond laser pulses," Appl. Phys. B **68**, 281–284 (1999).
44. J. K. Ranka, A. L. Gaeta, A. Baltuska, M. S. Pshenichnikov, and D. A. Wiersma, "Autocorrelation measurement of 6-fs pulses based on the two-photon-induced photocurrent in a GaAsP photodiode," Opt. Lett. **22**, 1344–1346 (1997).
45. S. Lochbrunner, P. Huppmann, and E. Riedle, "Crosscorrelation measurements of ultrashort visible pulses: comparison between nonlinear crystals and SiC photodiodes," Opt. Commun. **184**, 321–328 (2000).
46. J. Extermann, L. Bonacina, F. Courvoisier, D. Kiselev, Y. Mugnier, R. Le Dantec, C. Galez, and J.-P. Wolf, "Nano-FROG: frequency resolved optical gating by a nanometric object," Opt. Express **16**, 10405–10411 (2008).
47. P. Wnuk, L. L. Xuan, A. Slablab, C. Tard, S. Perruchas, T. Gacoin, J.-F. Roch, D. Chauvat, and C. Radzewicz, "Coherent nonlinear emission from a single KTP nanoparticle with broadband femtosecond pulses," Opt. Express **17**, 4652–4658 (2009).
48. N. Accanto, J. B. Nieder, L. Piatkowski, M. Castro-Lopez, F. Pastorelli, D. Brinks, and N. F. van Hulst, "Phase control of femtosecond pulses on the nanoscale using second harmonic nanoparticles," Light Sci. Appl. **3**, e143 (2014).
49. A. M. Larson and A. T. Yeh, "Ex vivo characterization of sub-10-fs pulses," Opt. Lett. **31**, 1681–1683 (2006).

1. Introduction

When a broadband, ultrashort laser pulse is focused with a lens, it gets distorted both in space and in time due to material dispersion as well as optical aberrations. Thus, broadband experiments place strong constraints on the experimental setup, especially if the investigated structures are small and lenses with high magnification have to be used.

Conventional high-numerical-aperture (high-NA) objectives are assemblies of glass lenses of total thickness of several centimeters and therefore they introduce large chromatic dispersion that has to be pre-compensated either by a pulse shaper or by a carefully chosen combination of prisms and chirped mirrors [1, 2]. All-reflective objectives do not suffer from dispersion, but have at most numerical apertures around 1 [3, 4].

An even more severe problem is the radial dependence of dispersion of a lens [5]. The rays passing the lens at different distances from the optical axis encounter different amounts of glass and experience different dispersion. As a result, the pulse arrival time and temporal shape depend on the position within the focus. When the measured signal depends on the electric field averaged over the entire area of the focus, these effects increase the effective duration of the pulse and decrease the temporal resolution. If the investigated structures are comparable in size to the focus diameter, spatial aberrations might lead to artifacts in the measurement as different parts of the system will interact with electric fields of different spectral phase and amplitude.

Pulse shapers offer not only a convenient method for pulse compression and characterization, but enable generation of shaped pulses as well as collinear, interferometrically stable pulse sequences. The ability to control ultrashort laser pulses combined with high spatial resolution is used in a variety of experiments, including selective nonlinear microscopy [6, 7], coherent control and coherent two-dimensional spectroscopy of plasmonic nanostructures [8–12], observation of energy transfer in single light-harvesting complexes [13], and many others. However, although a pulse shaper opens up new possibilites, it is also a further source of spatial beam profile distortions. In a spatial light modulator (SLM), if the phase of a spectral component of the pulse is changed, the wavefront of the pulse changes as well. This effect, known as space–time coupling, has been discussed theoretically as early as 1996 [14]. Further theoretical and

#223677 - $15.00 USD Received 23 Sep 2014; revised 18 Nov 2014; accepted 20 Nov 2014; published 12 Dec 2014

experimental studies investigating space–time coupling and other pulse-shaper artifacts, as well as comparing different pulse shaper configurations, followed [15–22].

Ultrafast experiments in general require information about the spectral phase and amplitude of the electric field at the point of interaction with the system of interest. Ray-tracing calculations could in principle provide information about the spatial profile in the focus volume of a microscope objective, but they would require an exact knowledge of the entire optical setup, including all material properties of the microscope objective lens. Therefore an experimental determination of spatiotemporal characteristics of the field in the focus is desirable. Existing experimental studies [23,24] contain valuable data about the order of magnitude of the expected effects as well as a comparison between different lenses, but most of the presented methods rely on characterizing a recollimated beam after it passed the same lens twice.

Several methods for pulse characterization directly in the focus of a lens have been proposed. One of them, suitable for full spatiotemporal characterization of a focused pulse, is a modified version of SEA TADPOLE, or Spatially Encoded Arrangement for Temporal Analysis by Dispersing a Pair of Light E-fields [25]. It makes use of a single-mode fiber with 5.6 μm mode diameter that is scanned within the focus volume. The pulse to be characterized is then overlapped with a known reference pulse coupled into a second fiber and the position-dependent temporal shape of the unknown pulse is measured using spectral interference. The fiber was later replaced with a near-field scanning optical microscopy (NSOM) probe which enabled sub-micron spatial resolution [26]. However, the authors note that the difficulty of maintaining interferometric stability of the setup causes blurring of the spatial component of the pulse phase.

Nanoparticles have been applied to characterization of spatiotemporal pulse distortions caused by pulse shaping [22]. The method relies on comparing the pump–probe fluorescence signal measured for different positions of a particle within the laser focus. Its disadvantage is that it only provides qualitative information, useful for comparing different pulse shaper-configurations, but quantitative information about the distortions was not obtained.

In conclusion, there is still need for a quantitative, high-resolution, and easy-to-implement method for spatiotemporal characterization of ultrashort pulses in the focus of a high-NA objective.

In this paper we describe a setup consisting of a phase-and-amplitude pulse shaper and an optical microscope with an oil-immersion high-NA objective lens. We concentrate on the aspects that are most relevant to preserving a short duration and a spectrally uniform spatial profile of the output beam. We compress the pulse in focus to under 10 fs, i.e., nearly to its Fourier limit. For this we use phase-resolved interferometric spectral modulation (PRISM), a shaper-assisted pulse compression method that is especially suited for compression of broadband pulses in a tight focus because it does not require second-harmonic generation [27]. Finally, we analyze experimentally the influence of optical aberrations and pulse-shaper space–time coupling on the spatiotemporal shape of the focus. For this, we introduce a new characterization method that uses nanostructures to achieve spatial resolution below the diffraction limit. We are able to show that in a carefully designed and aligned setup the spatiotemporal distortions caused by aberrations and space–time coupling are small. For shaped pulses the relative focus position shift of different spectral components is of the order of 10 nm and the pulse-arrival-time variation across the focus of the order of 1 fs, which is one order of magnitude less than the diffraction-limited focus size and the pulse duration, respectively.

2. Setup

The $4f$ pulse shaper described in this work is based on a design introduced already in 1983 [28]. This configuration, later extended by using programmable liquid crystal modulators first for

#223677 - $15.00 USD Received 23 Sep 2014; revised 18 Nov 2014; accepted 20 Nov 2014; published 12 Dec 2014

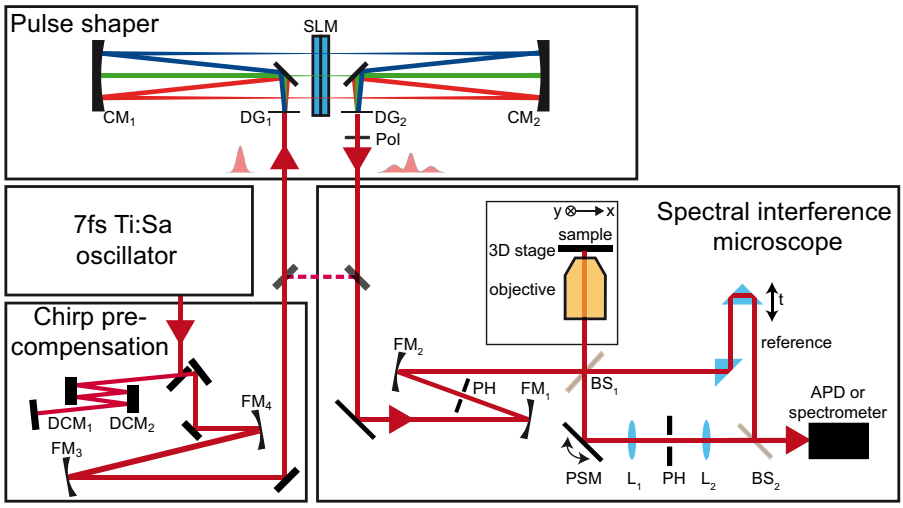

Fig. 1. Experimental setup: sub-10-fs pulses from a femtosecond oscillator (Venteon Pulse One PE) pass through a pulse shaper consisting of a spatial light modulator (Jenoptik SLM640d) in a $4f$ setup and are coupled into a spectral-interference microscope. DCM = dispersion compensating mirror (Venteon, DCM7), DG = diffraction grating (Wasatch Photonics, 600 lines/mm), CM = cylindrical mirror (Hellma Optik, $f = 300$ mm), Pol = polarizer (Thorlabs, LPVIS050), FM = focusing mirror , PH = pinhole, BS_1 = broadband 50/50 beamsplitter (Venteon), BS_2 = recombination beamsplitter, L = lens, PSM = piezo scanning mirror, APD = avalanche photodiode. For simplicity, the setup is pictured as flat, although in fact the beam is reflected upwards by 90° before entering the objective which is mounted vertically under the 3D stage.

phase [29] and then for phase-and-amplitude shaping [30], is well known and widely used [31, 32]. Due to its versatility it has been adapted for many applications, including shaping of broadband, sub-10-fs pulses [33, 34]. The specific configuration presented here – that is, the placement of folding mirrors and the angles between the beams – has been optimized by ray-tracing calculations to minimize the influence of optical aberrations. Details can be found in Appendix A.

The experimental setup is shown in Fig. 1. The pulses generated by a femtosecond oscillator pass a $4f$ pulse shaper with a 640-pixel liquid-crystal SLM placed in the Fourier plane. In principle such a setup produces phase- and polarization-shaped pulses. A polarizer after the second diffraction grating enables amplitude shaping by selecting one polarization component (in this case, p). The volume-phase-holographic gratings were designed for high efficiency in the spectral range between 650 nm and 950 nm. The specified diffraction efficiency varies from 90% at 800 nm to 70% at the edges of the spectrum. This variation causes a slight narrowing of the pulse spectrum, but still enables transmission of a broad bandwidth. The spectral resolution of the pulse shaper is 0.53 nm/pixel. According to the Nyquist theorem this determine the maximum temporal shift of the pulse which in this case is ± 1.9 ps. Similarly, the maximum second-order spectral phase can be estimated to be about ± 5000 fs^2.

In principle the pulse shaper can be used to compensate for the chromatic dispersion of the optical elements including the objective lens by applying a phase of equal magnitude, but opposite sign than the phase accumulated by the pulse as a result of dispersion. However, if sub-10-fs pulses are used, one should take care to minimize the dispersion of the setup by using reflective elements where possible and thin elements in other cases to avoid using the entire shaping

#223677 - $15.00 USD Received 23 Sep 2014; revised 18 Nov 2014; accepted 20 Nov 2014; published 12 Dec 2014

window merely for compensating the dispersion. We use custom-made 1-mm-thin diffraction gratings and a 2-mm-thin polarizer. Finally, the pulses are prechirped with several bounces on a pair of dispersion compensating mirrors to reduce the chirp that has to be applied by the pulse shaper. As the microscope alone introduces about 2800 fs^2, precompensating the entire quadratic phase of the pulse in the focus would require more than 20 reflections per mirror. Apart from alignment difficulties, that many reflections cause losses. We also observed some beam profile distortions that seem to originate from the mirrors not being completely uniform over their entire surface area. For this reason we decided to use a moderate number of reflections (8 per mirror) as a compromise.

Following chirp precompensation and pulse shaping the beam is coupled into a spectral interference microscope setup, that is, a confocal microscope with a reference beam path for spectral interference measurements. The setup was previously described in detail [35]. Briefly, a Keplerian telescope is used to adjust the beam size to fill the back aperture of the microscope objective. To adapt the telescope for broadband pulses, the lenses were replaced with spherical mirrors (FM_1 and FM_2 in Fig. 1). More importantly, a 100-µm pinhole in the focus of the telescope cleans the beam profile and ensures reproducible day-to-day incoupling. Next, the beam is divided by a broadband beamsplitter. One part of the beam is focused on the sample using an immersion-oil objective (Nikon Plan Apo, 100×, NA 1.4). The other part of the beam is used as a reference for spectral interference measurements. All measurements presented in this paper were taken in the confocal configuration, using a second telescope with a pinhole in the focal plane of the signal path. This has to be taken into account while comparing the measured focus sizes with the diffraction limit (see section 4.3 in [36]). Finally, both beams are recombined on a beamsplitter (BS_2 in Fig. 1) and directed either to an avalanche photodiode or into a high-resolution, low-noise spectrometer (see [35] for details).

3. Temporal compression and characterization

Although high-NA-focused 10-fs pulses compressed by conventional optics have been demonstrated [2], compression of very broadband pulses to their Fourier limit requires correcting for higher-order chromatic dispersion. This is conveniently achieved with a pulse shaper that can be also employed to simplify pulse characterization by reducing the number of optical elements in the setup and eliminating the spatial and temporal overlap noise. Many pulse-shaper-based techniques for characterization exist, mostly relying on generating multiple pulse shapes and measuring a nonlinear signal. For example, the pulse shaper can be used to generate a pulse pair with variable delay to obtain an interferometric autocorrelation or interferometric frequency-resolved optical gating (FROG) trace [37–39]. Another widely used method is multiphoton intrapulse interference phase scan (MIIPS) [40] which has the advantage of requiring only phase modulation, and not phase-and-amplitude modulation like FROG.

Methods such as FROG and MIIPS rely on second-harmonic generation (SHG) and evaluation of the SH spectra. Another, experimentally simpler approach makes use of the fact that the efficiency of a broadband nonlinear process is maximized if the pulse is transform-limited. A search algorithm using the intensity of a nonlinear signal as feedback finds the spectral phase that produces a transform-limited pulse after the pulse shaper. Due to the large amount of degrees of freedom evolutionary algorithms and simulated annealing, among others, have been used for automated pulse compression [41–43]. As a nonlinear process one can use the integrated second-harmonic intensity, but other nonlinear processes, such as two-photon-induced photocurrent, have been shown to yield equivalent results [44, 45].

All these methods can in principle be applied to compress a tightly focused pulse. In some cases tight focusing makes the measurement easier since the peak power and the efficiency of the nonlinear process increase. Furthermore, by using a single nanocrystal as nonlinear medium

#223677 - $15.00 USD Received 23 Sep 2014; revised 18 Nov 2014; accepted 20 Nov 2014; published 12 Dec 2014

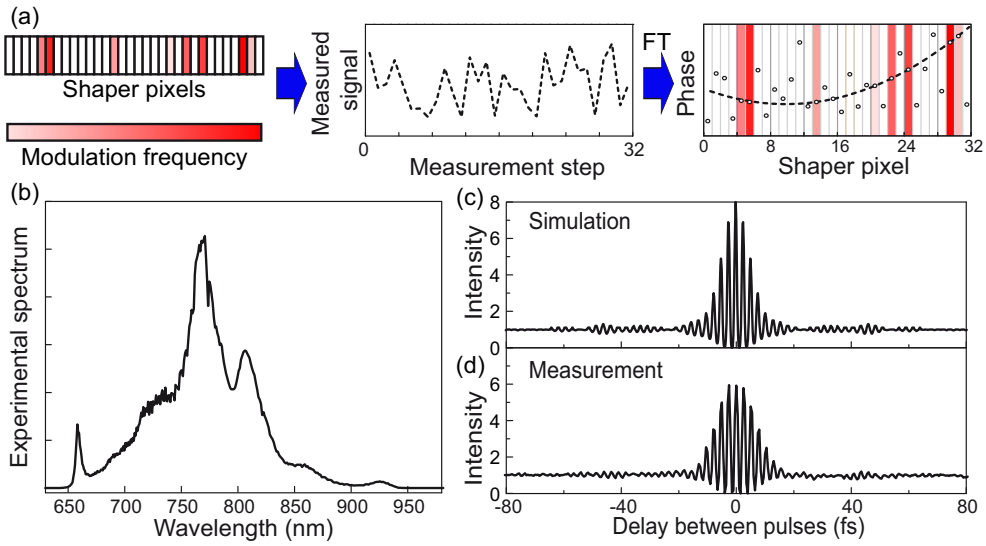

Fig. 2. (a) Principle of the PRISM algorithm. (Left panel) $n/4$ pixels are selected and modulated with specific frequencies marked in shades of red. (Middle panel) With each of the $n/4$ modulation steps the nonlinear signal is measured. (Right panel) After a Fourier transformation (FT) the phase values (circles) for the $n/4$ pixels are extracted from the Fourier transform of the signal. The phase to be found is marked with a dashed line. Same procedure is repeated for the other three groups until all n spectral components are found. (b) Spectrum of the compressed pulse in the focal plane, obtained by measurement before the microscope objective and multiplying by objective transmission. (c) Interferometric autocorrelation trace simulated by using the experimentally measured spectrum and assuming flat spectral phase. (d) Interferometric autocorrelation trace measured in the focus (see text for details).

the measurement can be performed with sub-micrometer resolution [46–48]. However, applying FROG or MIIPS to the compression of broadband pulses in the focus of a high-NA objective is challenging because it requires collecting of broadband UV radiation that is typically not transmitted by microscope objectives designed for the visible or near infrared. Measuring the integrated intensity is usually easier. A wide variety of materials can be used to generate the feedback signal, provided that they exhibit two-photon absorption or facilitate SHG in the investigated spectral region. For example, second-harmonic upconversion of the ultrashort pulse spectrum within collagen in a mouse tail tendon has been used for compression and characterization of sub-10-fs pulses [49].

The algorithm we use in this work, phase-resolved interferometric spectral modulation (PRISM) [27], is relatively new in the ultrashort community. It was originally proposed for optimization of the spatial phase of a beam propagating through scattering media and then applied to the spectral phase of ultrashort pulses [27]. The principle of the PRISM algorithm is illustrated in Fig. 2(a). Unlike in most evolutionary algorithms, the pixels are not modulated randomly, but with certain unique frequencies. The collected signal is Fourier-transformed to extract the contribution of each pixel. The principle is similar to that of a lock-in amplifier, but the frequency filtering is done digitally. Moreover, the signal is modulated with many frequencies at once which significantly shortens the measurement. An advantage of this algorithm is that it does not require making any assumptions about the phase of the pulse – even phase jumps can be found.

#223677 - $15.00 USD Received 23 Sep 2014; revised 18 Nov 2014; accepted 20 Nov 2014; published 12 Dec 2014

To compress the pulse we used four iterations of the algorithm. During each iteration the pixels were divided into four groups and the groups were modulated one at the time, while the phase of the remaining three stayed constant. In the first two iterations, neighboring pixels were bunched into groups of four to increase the sensitivity and speed. This way, an approximation of the compensation phase could be found quickly. The last two iterations were performed with full resolution. As a feedback signal, we used the photoinduced current of a GaAsP photodiode (G5645 Hamamatsu) placed directly in the focused beam after the objective lens. Because of the short working distance of the objective, a part of the diode casing had to be carefully removed so that the photosensitive surface could be placed closer to the lens (because of the thickness of the protective coating the sensor was still slightly out of the focal plane).

The compressed pulse was characterized using shaper-assisted interferometric autocorrelation measured with the same photodiode that was used for PRISM. Interferometric autocorrelation does not provide a full information about the pulse spectral phase. To verify whether the pulse is compressed, we numerically calculated the autocorrelation trace of a perfectly compressed pulse by taking the measured spectral intensity as shown in Fig. 2(b) and assuming flat spectral phase. The simulated trace is shown in Fig. 2(c) and the measurement in Fig. 2(d). The measured pulse duration is 9.3 fs which is close to the Fourier limit of 7.6 fs. The duration was obtained by numerically filtering out the oscillating component, fitting a Gaussian and taking its full width at half maximum.

A collinear FROG trace was also measured using nanocrystals (Barium titanate(IV) nanopowder, 467634-25G, Sigma Aldrich) for SHG and a lens to collect the SH signal in transmission configuration. However, the signal-to-noise ratio in the tails of the spectrum was not sufficient to fully retrieve the spectral phase and amplitude of the pulse; increasing the pulse energy resulted in damaging the nanocrystals.

4. Spatial characterization of the focus

In order to characterize the spatiotemporal pulse shape in the focus, we introduce a new, all-optical and easy-to-use method suitable for high-NA focused laser beams. We employ a nanoparticle as a nano-scatterer, reflecting only a selected part of the laser focus. This concept is shown schematically in Fig. 3(a). The structures are gold nanorods with 34 nm length and 25 nm diameter (Nanopartz). Their 550-nm resonance wavelength is outside the laser spectrum [shown in Fig. 2(b)], so their spectral response is flat. The principle of this measurement is similar to the scanning SEA TADPOLE [26], but using commercially available nanostructures as probes makes the experimental setup simpler. At the same time the spatial resolution is significantly higher than in a setup using a single-mode fiber or even an NSOM tip.

Before the measurement the nanorods are distributed on a microscope cover-glass marker structure. To reduce the background from the glass–air interface reflection, we place a drop of immersion oil with matching refractive index on the glass surface. To ensure that only single nanorods, and not clusters, are selected for the measurement the optical image is compared to a scanning electron microscope (SEM) image. In addition, we compared the results from several different nanorods to make sure that their orientation has no influence on the measurement. Finally, since the measurements presented below are linear in intensity, we could easily obtain sufficient signal-to-noise ratio with relatively low intensities. For the measurements shown below the average power in focus was 60 μW. This could be still increased by about one order of magnitude without damaging the nanorods.

Using this method, we first characterized the beam coupled into the microscope setup without passing the pulse shaper (dashed line in Fig. 1) by scanning a nanoparticle in the focal plane in 40-nm steps and measuring the reflected spectrum for each point. The results are shown in Figs. 3(b)–3(d). In the following, we define the *x* direction as the one parallel to the beam polarization

#223677 - $15.00 USD Received 23 Sep 2014; revised 18 Nov 2014; accepted 20 Nov 2014; published 12 Dec 2014

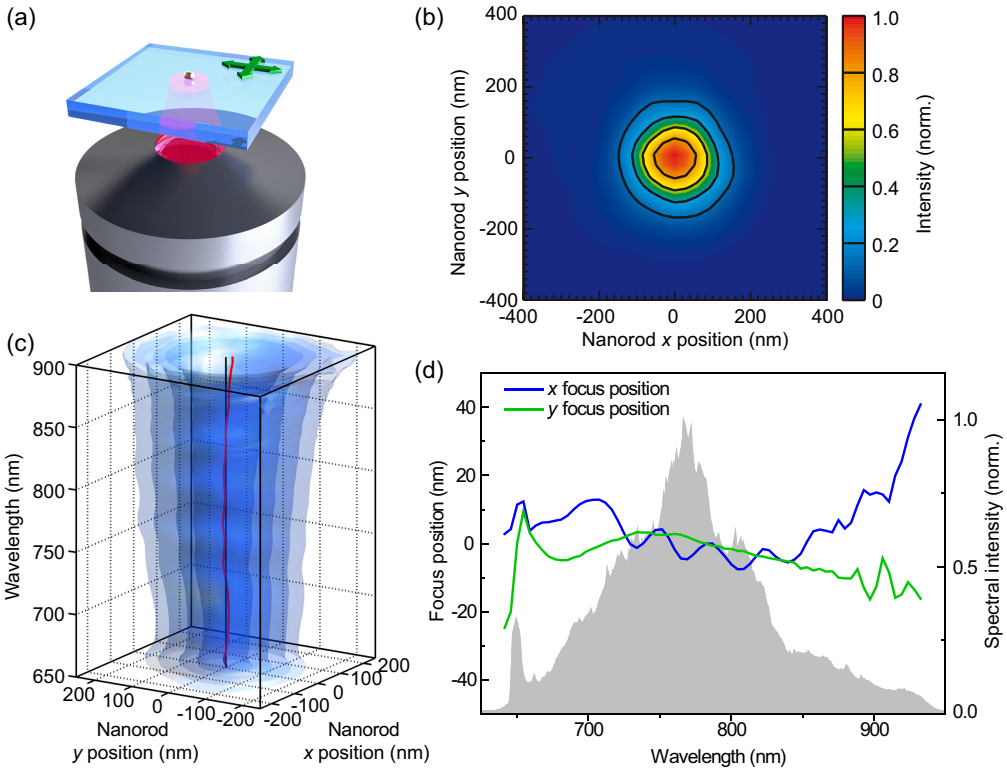

Fig. 3. Spatial characterization of a tightly focused beam. (a) Principle: a nanoscatterer is scanned in the focal plane of the microscope objective. (b) Spectrally integrated and (c) spectrally resolved back-reflected intensity. The red line in (c) indicates the center position for each wavelength as obtained from a 2D Gaussian fit of the intensity distribution, the black line marks the zero position, and the blue 3D contours correspond to $6/e^2$, $4/e^2$, $2/e^2$, and $1/e^2$ of the maximal intensity for each wavelength. (d) Wavelength-dependent focus position, i.e., the x (blue) and y (green) coordinates of the red line from (c). The pulse spectrum in the focal plane (with the objective transmission taken into account) is shown in gray.

#223677 - $15.00 USD Received 23 Sep 2014; revised 18 Nov 2014; accepted 20 Nov 2014; published 12 Dec 2014

and to the pulse shaper spectral axis. From the spectrally integrated signal in Fig. 3(b) it can be seen that the beam is focused to a small, round spot, but since the signal is averaged over almost 300 nm of spectral range, spatial chirp in a given direction cannot be distinguished from a beam that is elongated in this direction but spectrally homogeneous.

More information can be extracted from the spectrally resolved back-reflected intensity as visualized in Fig. 3(c). As expected, the size of the focus increases with the wavelength. Secondly, it can be seen that the focus position is different for different spectral components, but the displacement is much smaller than the size of the focus. To quantify that, a two-dimensional Gaussian intensity distribution was fitted to the data for each spectral component separately. In the following, the center of this fit will be referred to as the wavelength-dependent focus position, shown as a red line in Fig. 3(c) and again in Fig. 3(d) as two lines for the x and y directions. In the region between 700 and 850 nm, where most of the spectral intensity is concentrated, the deviations from the position of the center wavelength are smaller than 10 nm. Since these data were taken for a beam coupled into the microscope without passing the pulse shaper, these deviations can only be caused by an inherent spatial chirp of the laser output or introduced by the remaining optics and imperfect incoupling into the microscope. In particular, we attribute the oscillation along the x direction to the influence of the chirped mirrors.

A deviation of 10 nm might seem large compared to the size of some nanoparticles. However, for a Gaussian beam of 240-nm radius (the diffraction-limited size for 800 nm and objective lens with NA of 1.4 for the confocal detection case), a shift by 10 nm corresponds to a change of intensity by less than 0.5% for the point in the center of the beam and maximally 8% for the point where the Gaussian distribution has the steepest slope. This means that the effective spectrum interacting with a nanoparticle is slightly position-dependent, but as long as the deviations are small in comparison to the focus size and remain constant during a measurement series, they are not detrimental to the experiment.

Our characterization method enables us also to extract the spatial phase in the focus with subdiffraction spatial resolution. For this, for each nanorod position the back-reflected beam was overlapped with a reference beam and the spectral interference pattern was measured. This way, the spatial variation of the pulse arrival time in the focal plane could be measured. The results are shown in Fig. 4(a). It is visible how the pulse arrival time depends on the distance from the centre of the beam. This can be attributed to the radial chirp introduced by the objective. For a quantitative analysis of these results, it has to be taken into account that the characterized light passes through the objective twice. Assuming that the distortion of the wave front is identical for propagation in both directions, the actual arrival time in the focal plane can be obtained by dividing the measured time that is shown in Fig. 4(a) by 2. The red dashed line indicates the beam size (that is, the contour line corresponding to $1/e^2$ of the maximal intensity). The pulse front is almost flat, with a small tilt of about 1 fs.

Since many nanostructures are very thin, typically only the arrival time in the focal plane is relevant for the experiment. However, our method can be used for characterization of the entire focus volume. As an example, measurements in two planes further away and closer to the objective lens than the focal plane are shown in Figs. 4(b) and 4(c), respectively. It is visible how the pulse front curves further as the beam propagates, as expected.

Finally, it has to be noted that the spatial chirp in the focus is very sensitive to the incoupling into the microscope objective. The achromatic objective lenses are optimized for beams coupled perfectly along the optical axis, but even a small misalignment leads to a strong wavelength dependence of the focus position. One indication of correct incoupling is the pattern that appears if the reflection of a strongly focused polarized beam is observed through a second polarizer [36], but since the beam entering the objective has two degrees of freedom – position and angle – one parameter is not sufficient to adjust both of them. We optimized the incoupling

#223677 - $15.00 USD Received 23 Sep 2014; revised 18 Nov 2014; accepted 20 Nov 2014; published 12 Dec 2014

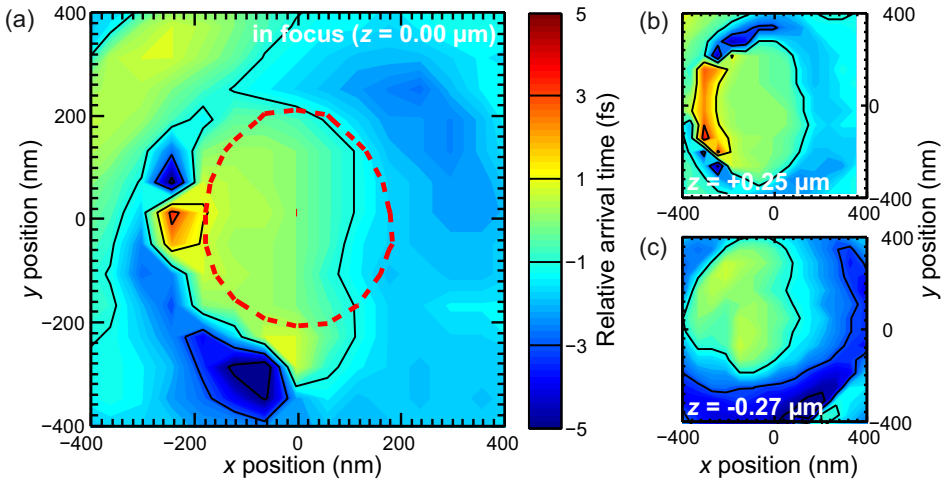

Fig. 4. Position-dependent pulse arrival time obtained by spectral interferometry (a) in the focal plane of the objective as well as in two planes (b) further away and (c) closer to the objective lens. The time corresponds to two passes through the objective. Red dashed line: $1/e^2$ of the maximal intensity contour line.

using the spatial chirp measured with a nanorod as the second observable. This procedure is time-consuming, as it has to be done iteratively with measurements after every step, but it has to be done only once, or if significant changes are made to the setup. Before optimization, the beam exhibited a significant residual linear spatial chirp (about 60 nm shift of the blue edge relative to the red edge of the spectrum) that was difficult to measure by other methods. The result shown in Fig. 4 was obtained after optimized incoupling, showing the significance of the characterization method demonstrated here.

5. Influence of pulse shaping on the focus

Pulse shapers influence the beam profile in several ways. Firstly, even a perfectly aligned $4f$ setup exhibits some optical aberrations. Furthermore, due to space–time coupling, the spatial beam profile depends on the temporal shape of the pulse. In this section we investigate the influence of the pulse shape applied by the SLM on the wavelength-dependent focus position. We consider both pure phase masks and phase-and-amplitude masks. We do not explicitly investigate phase steps, but due to phase wrapping phase jumps of 2π are present in all investigated masks.

First, we take a look at the simplest example, a linear spectral phase that results in a shift of the pulse in the time domain. Since in many experiments a compressed pulse in the focal plane is desired, in the following we add an offset phase for dispersion compensation (determined by PRISM) to the spectral phase applied by the shaper.

The wavelength-dependent focus position was determined, as described in detail in the previous section and Fig. 3, for pulses with time delays of -200 fs, 0 fs, and 200 fs. To minimize the influence of the finite accuracy of the sample positioning unit (in particular, the repeatability which is about 5 nm), we were measuring all pulse shapes in a row for every position, rather than set one pulse shape, scan the position, and repeat it for the next pulse shape. The measurement results are shown in Fig. 5. The wavelength-dependent focus position in the *x* and *y* direction is shown in Figs. 5(a) and 5(b), respectively. The changes of the position are slightly larger than for the beam bypassing the shaper [Fig. 3(d)]. The steep slope for the wavelengths

#223677 - $15.00 USD Received 23 Sep 2014; revised 18 Nov 2014; accepted 20 Nov 2014; published 12 Dec 2014

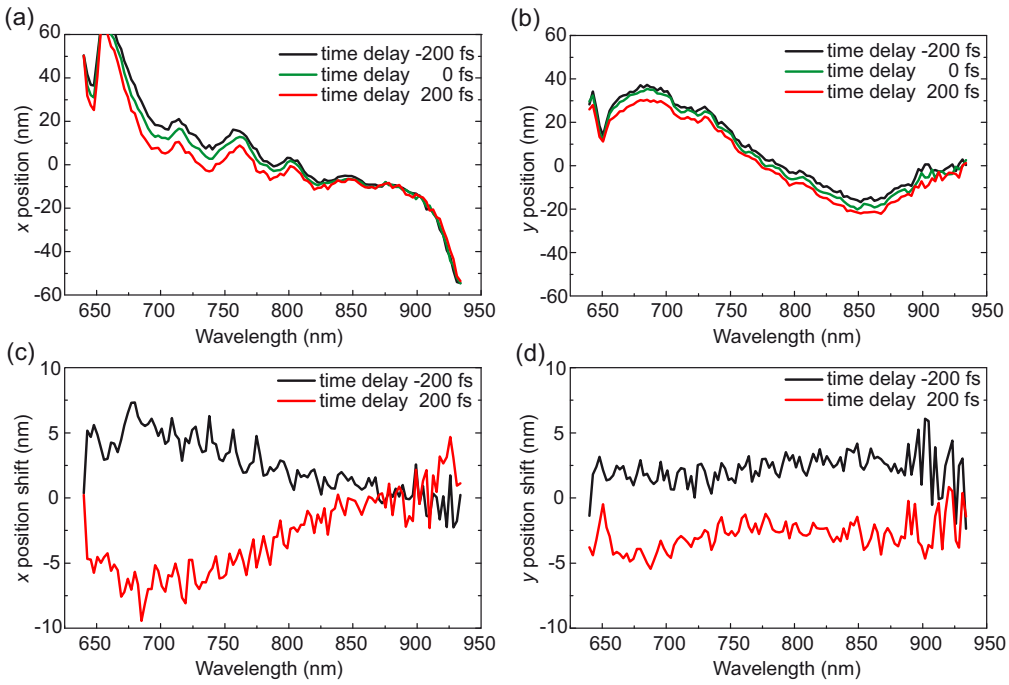

Fig. 5. Wavelength-dependent (a) *x* and (b) *y* focus position for pulses with an offset phase for dispersion compensation and time delays of -200 fs (black), 0 fs (green), and 200 fs (red) introduced by the pulse shaper. (c) Shift of focus position in *x* and (d) *y* direction relative to the compressed pulse with a delay of 0 fs.

at the edges of the pulse spectrum can be attributed to the influence of the $4f$ telescope. Due to spherical aberrations, the focal length depends on the distance of the beam from the optical axis.

To quantify how the focus shifts when a spectral phase is applied – which is the parameter that actually matters in a coherent control experiment – the shift relative to the 0-fs-delay pulse was calculated and is shown in Figs. 5(c) and 5(d) for the *x* and *y* direction, respectively. Since no changes or adjustments were made to the setup in between the measurements for each pulse shape, this shift is caused only by space-time coupling, that is, the change of the beam path in space caused by modulating its temporal shape. For most wavelengths the shift is less than 5 nm, which is small compared to the focus size. Furthermore, we repeated the arrival time measurement (not shown) and determined that the results are essentially the same as for pulses bypassing the shaper, which confirms that the arrival time variation is caused mostly by propagation through the objective lens. For comparison, we also repeated the measurements for pulses with different time delays, but without dispersion compensation phase (not shown). The position shifts caused by a given time delay for the compressed and uncompressed pulse are very similar.

To investigate if the observed position shift increases with increasing time delay applied with the shaper, we measured the wavelength-dependent focus position for delays of ± 1 ps and ± 2 ps (see Fig. 8 in Appendix B). In this case the maximal shift of the focus position with respect to the unshaped pulse is about 15 nm, so only by a factor of 3 larger than that in Fig. 5, although the time delay increased by an order of magnitude.

Due to several different sources of pulse-shaper artifacts it is difficult to predict the amount

#223677 - $15.00 USD Received 23 Sep 2014; revised 18 Nov 2014; accepted 20 Nov 2014; published 12 Dec 2014

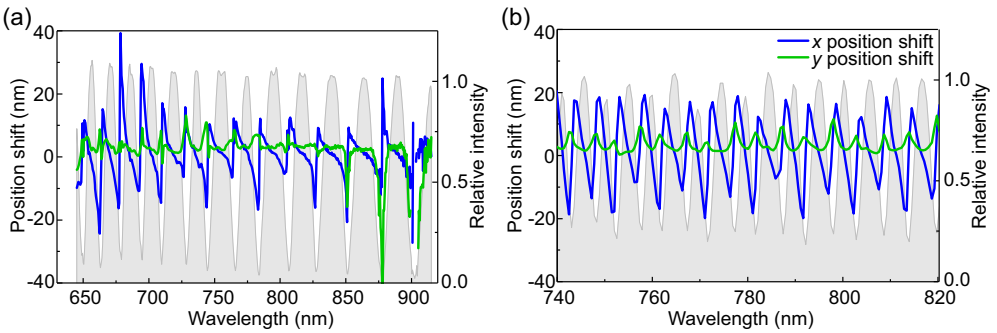

Fig. 6. Shift of the x (blue) and y (green) wavelength-dependent focus position for pulse pairs with a delay of (a) 100 fs and (b) 400 fs. In (b), only part of the spectral range is shown for clarity. The pulse-pair spectrum divided by the spectrum of a single pulse is shown in grey.

of space–time coupling in a given experiment. Some authors find that space–time coupling vanishes in the focal plane for pure phase masks [18], while others point out that this is the case at the geometrical focus position and not the effective focus position where the beam waist is smallest [17, 20]. We find that some dependence of the focus shape on the spectral phase is present. However, the shift of the focus position is not proportional to the slope of the phase, as it is the case for collimated beams [18], but reaches a certain maximal value. Although a linear spectral phase is only one of many possible phase masks, it can be expected that results for other phase masks will be similar, as all smooth phases can be approximated by a chain of line segments.

Apart from pure phase masks, phase-and-amplitude masks are also used in coherent control experiments. A common example of a pulse shape that requires amplitude shaping is a double pulse with variable time delay generated by applying a periodic amplitude mask. A frequently mentioned advantage of using a pulse shaper to generate pulse pairs is that the lack of moving parts in the pulse shaper guarantees spatial overlap of both pulses, but this is strictly true only in the absence of space–time coupling. We measured the wavelength-dependent focus position for pulse pairs with different time delays and show the results for double pulses separated by 100 fs [Fig. 6(a)] and 400 fs [Fig. 6(b)]. It is apparent that a periodic mask causes a periodic distortion. To give a better idea on how the focus shift is correlated to the transmission mask, we also plotted the measured ratio of the spectral amplitude of a pulse pair to that of a single pulse. It is apparent that the spectral components with the largest shift are those with the smallest intensity.

If the two pulses in a pulse pair are slightly displaced, then they propagate differently through the microscope objective which in principle can influence the time delay between them. The actual time delay can be deduced from the period of the interference fringes in the position-dependent spectra. In Fig. 7 the measurement of the position-dependent time delay is shown for the double pulse with separation 400 fs (for the pulse with separation 100 fs there are not enough interference fringes to achieve sufficient precision). The measured variation of the delay across the focus is $< \pm 1$ fs and thus is small compared to the pulse duration.

6. Summary

In summary, we have demonstrated a setup that combines a high-NA oil-immersion objective with a broadband pulse shaper. The pulses have been compressed in the focal plane to a

#223677 - $15.00 USD Received 23 Sep 2014; revised 18 Nov 2014; accepted 20 Nov 2014; published 12 Dec 2014

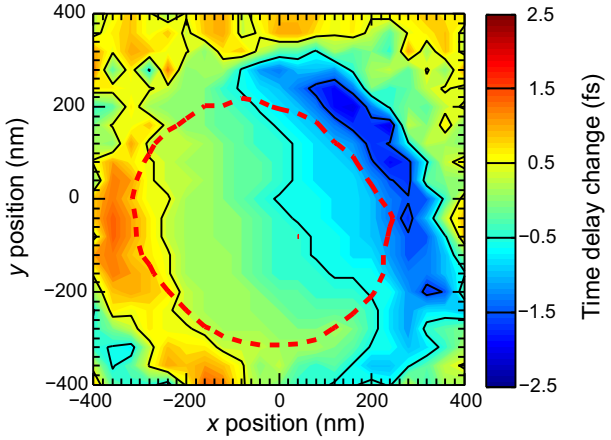

Fig. 7. Position-dependent variation of temporal separation of two pulses in a pulse pair relative to the value of 400 fs set by the pulse shaper (for clarity, the scale is different than in Fig. 4). Red dashed line: $1/e^2$ of the maximal intensity contour line.

sub-10-fs duration using a shaper-assisted algorithm, PRISM. Further, we have experimentally characterized the influence of the optical aberrations caused by the objective lens and the $4f$ setup as well as space–time coupling on the spatiotemporal focus profile. For this, we developed a new method that utilizes a gold nanorod as a probe. Due to its simplicity, this method can be applied in any setup capable of position-sensitive detection. The measured position-dependent deviation of the pulse arrival time is less than 1 fs across the focus. We have further shown that a carefully designed and aligned single-pass $4f$-setup-based pulse shaper exhibits a wavelength-dependent focus position shift of less than 15 nm, which is small compared to the diffraction-limited focus size. This makes the presented setup suited for demanding applications such as coherent control or time-resolved spectroscopy on the nanoscale.

Appendix A: Pulse-shaper design

Even a perfectly aligned pulse shaper does not leave the spatiotemporal profile of the beam unchanged. Due to the spherical aberration of the cylindrical mirrors (the same is true for cylindrical lenses) the effective focal length depends on the distance from the optical axis so it is different for different spectral components of the pulse. Moreover, in the configuration we chose the beams do not lie in one plane. Specifically, the mirror that couples the beam into the pulse shaper is tilted upwards so that the beam travels at a constant angle to the table surface (less than 3° in our case) until it hits the cylindrical mirror (it is horizontal between the cylindrical mirrors). As a result, in the output beam the wavelengths on the edges of the spectrum are displaced vertically from the central wavelength. One alternative would be entering the reflective telescope from the side, but hitting the cylindrical mirror off-axis would cause coma. We performed ray-tracing calculations using the Optica package for Mathematica and determined that the aberrations resulting from the vertical tilt are expected to be smaller than those in the off-axis configuration for a given focal length of the focusing mirror.

From the geometrical aberrations' point of view, the focal length of the mirrors should be as long as possible, since this allows a smaller input beam angle. However, for a given input beam size a larger focal length leads to a larger beam waist of a single spectral component in the Fourier plane. This limits the shaper resolution and increases the distortions of the output beam spatial profile [17]. The pixel size of the Jenoptik SLM is 100 µm×10 mm. The beam from the

#223677 - $15.00 USD Received 23 Sep 2014; revised 18 Nov 2014; accepted 20 Nov 2014; published 12 Dec 2014

laser is expanded to a $1/e^2$ diameter of 7 mm, so for a focal length of 300 mm the diameter of a single spectral component in the Fourier plane is 45 µm. Accordingly, 300 mm was chosen as a compromise.

Finally, we decided against using a configuration with a mirror placed after the second grating and the beam passing the entire $4f$ setup twice. Such a setup was first analyzed in [14]. The authors conclude that double-passing the apparatus cancels space–time coupling only for simple masks. A later paper [19] essentially confirms this result. In a recent paper [22] the calculation for space–time coupling in a double-pass pulse shaper was repeated, this time with a somewhat different conclusion. The authors note that although this configuration does not always eliminate space–time coupling, it reduces it leaving only higher-order terms. However, the double-pass configuration has other disadvantages, for example the loss and distortions caused by the $4f$ setup are doubled. The experimental results of our investigation presented in this paper show that a single-pass configuration works well.

Appendix B: Shift of focus position for larger time delays

To test the limits of the setup, the wavelength-dependent focus position for pulses with time delays of -2 ps, -1 ps, 1 ps and 2 ps was measured. Then the focus position shift was calculated by subtracting the 0 ps-shift curve [compare to Figs. 5(c) and 5(d)]. The results presented in Fig. 8 show that even for steep spectral phases the shift does not exceed ± 15 nm.

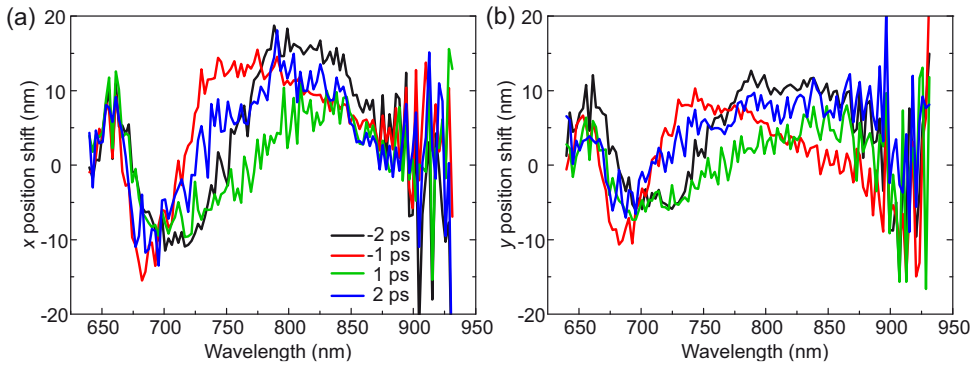

Fig. 8. (a) Shift of the wavelength-dependent focus position in x and (b) y direction for pulses with time delays of -2 ps (black), -1 ps (red), 1 ps (green), and 2 ps (blue) relative to the unshaped pulse with a shift of 0 ps.

Acknowledgments

This work was supported by the DFG within the Priority Program “Ultrafast Nanooptics” (SPP 1391) and the publication by the DFG and the University of Würzburg in the funding program “Open Access Publishing”.